Chemical Synthesis

Two-dimensional manganese oxide on ceria for the catalytic partial oxidation of hydrocarbons

Hai Wang[1], Liang Wang[1,*], Qingsong Luo[1], Jian Zhang[2], Chengtao Wang[3], Xin Ge[4], Wei Zhang[4,*], Feng-Shou Xiao[1,*]

[1]Key Lab of Biomass Chemical Engineering of Ministry of Education, College of Chemical and Biological Engineering, Zhejiang University, Hangzhou 310028, Zhejiang, China.
[2]Beijing Advanced Innovation Center for Soft Matter, Science, and Engineering, Beijing University of Chemical Technology, Beijing 100029, China.
[3]Key Laboratory of Applied Chemistry of Zhejiang Province and Department of Chemistry, Zhejiang University, Hangzhou 310028, Zhejiang, China.
[4]Key Laboratory of Automobile Materials MOE, School of Materials Science & Engineering, Jilin Provincial International Cooperation Key Laboratory of High-Efficiency Clean Energy Materials, Electron Microscopy Center, and International Center of Future Science, Jilin University, Changchun 130012, Jilin, China.

*Correspondence to: Prof. Liang Wang, Key Lab of Biomass Chemical Engineering of Ministry of Education, College of Chemical and Biological Engineering, Zhejiang University, Hangzhou 310028, Zhejiang, China. E-mail: liangwang@zju.edu.cn; Prof. Wei Zhang, Key Laboratory of Automobile Materials MOE, School of Materials Science & Engineering, Jilin Provincial International Cooperation Key Laboratory of High-Efficiency Clean Energy Materials, Electron Microscopy Center, and International Center of Future Science, Jilin University, Changchun 130012, Jilin, China. E-mail: weizhang@jlu.edu.cn; Prof. Feng-Shou Xiao, Key Lab of Biomass Chemical Engineering of Ministry of Education, College of Chemical and Biological Engineering, Zhejiang University, Hangzhou 310028, Zhejiang, China. E-mail: fsxiao@zju.edu.cn

Abstract

Although the rational synthesis of catalysts with strong oxide-support interactions to modulate the geometric and electronic structures and achieve unusual catalytic performance is challenging in heterogeneous catalysis, it is in significant demand for the efficient and sustainable transformation of chemicals. Here, we report the synthesis and performance of a ceria-supported two-dimensional manganese oxide catalyst with strong metal oxide-support interactions, which help to produce well-dispersed and amorphous MnO_x layers on the CeO_2 matrix (MnO_x/CeO_2). This catalyst readily reacts with molecular oxygen to give a high capacity of active oxygen species, owing to the interfacial effect. The C-H bonds are adsorbed and activated by these active interfacial oxygen species, leading to high activities and selectivities in the industrially important C-H bond activation reactions, such as the oxidation of hydrocarbons to alcohols and ketones with molecular oxygen under solvent- and initiator-free

conditions at mild temperature. The performance of the MnO_x/CeO_2 catalyst is greater than that of noble metal and highly efficient Mn-Ce solid-solution catalysts. More importantly, the catalyst is stable and exhibits constant reactivity in continuous recycling tests. These results are important for the design of highly efficient catalysts for the selective oxidation of hydrocarbons.

Keywords: Strong oxide-support interactions, C-H oxidation, MnO_x/CeO_2 catalyst, heterogeneous catalysis

INTRODUCTION

The oxidation of sp^3-hybridized C-H bonds has emerged as a facile and industrially important process for the sustainable production of alcohols, ketones and epoxides from petroleum hydrocarbons[1-4]. Generally, the inorganic salts of ClO_4^- and NO_3^- are used as oxidants, which are costly and environmentally unfriendly[5]. Although molecular oxygen is regarded as a favorable oxidant, harsh reaction conditions are necessary for the activation of strong C-H bonds, which generally leads to significant energy consumption and uncontrollable selectivities[6-9]. In addition, over-oxidation occurs in many cases to produce carbon dioxide and other byproducts, particularly during vapor-phase oxidation[3,10]. As an attractive process in industry, the liquid-phase oxidation of C-H bonds has attracted tremendous attention, but the conversion of hydrocarbon substrates is always unsatisfactory. Subsequently, noble metal catalysts, peroxide initiators, organic solvents, supercritical CO_2 and ionic liquid additives are used for enhancing the substrate conversion[11-16], but new problems arise, such as increased costs and extra product purification. Therefore, the efficient catalytic oxidation of C-H bonds with molecular oxygen over non-noble metal catalysts, as well as avoiding the use of solvents and initiator additives, remains challenging.

Mn-Ce oxides have been extensively investigated as efficient catalysts for the total oxidation of NO[17], CO[18-23] and organic molecules for pollutant removal[24-28], because of their high activity toward the activation of molecular oxygen. The features of Mn-Ce oxides in molecular oxygen activation have also motivated research into the selective oxidation of C-H bond and excellent success has been achieved. For example, Mn-Ce oxides were synthesized with surfactants or ionic liquids to maximize the solid-solution phase, which readily exhibited superior activity and selectivity for the selective oxidation of hydrocarbons[18]. However, organic solvents are still necessary in most of these cases[18]. Furthermore, the expensive surfactants and ionic liquids still limit their practical applications. Developing strategies for the synthesis of efficient Mn-Ce catalysts therefore remains a vital area of research in this field.
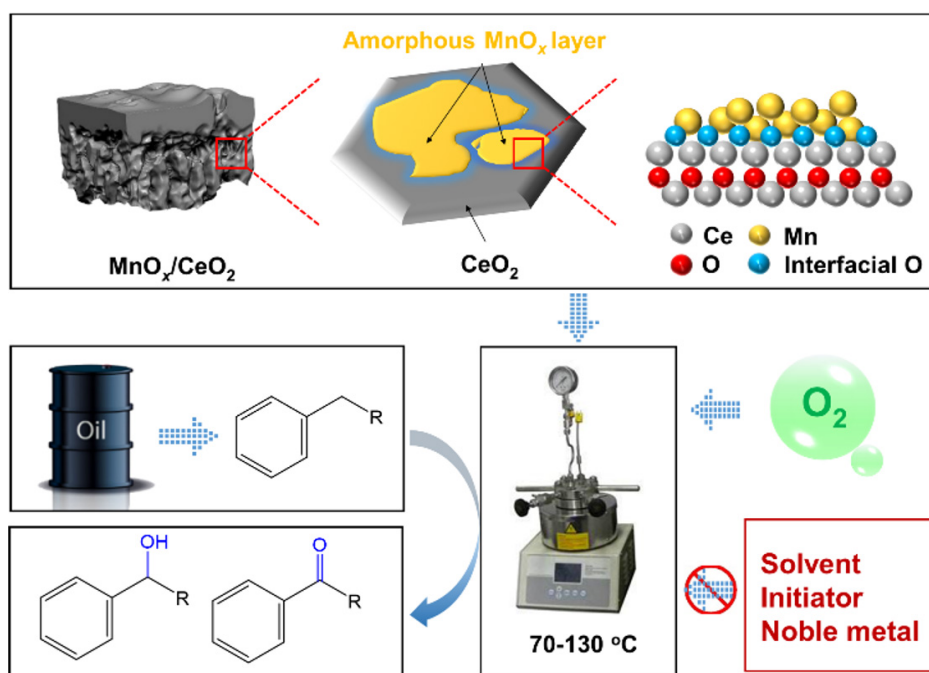
Here, we report a ceria-supported two-dimensional manganese oxide catalyst that is highly efficient for the selective oxidation of hydrocarbons without the use of solvents and initiator additives. The key to this success is anchoring the two-dimensional and amorphous manganese oxide layers on the cerium matrix (MnO_x/CeO_2) via strong oxide-support interactions (SOSIs). Owing to these features, the catalyst readily reacts with molecular oxygen to give a high capacity of active oxygen species at 46.1%. In the solvent- and initiator-free oxidation of C-H bonds on a series of hydrocarbons with molecular oxygen at low temperatures, the MnO_x/CeO_2 catalyst exhibits high activities and selectivities, as well as good stabilities in the recycling tests (Scheme 1). For example, in the aerobic oxidation of ethylbenzene, it gives a conversion of 63.5% and a selectivity of 95.7% to the corresponding alcohol/ketone products, thereby outperforming highly efficient heterogeneous catalysts under solvent- and initiator-free systems reported in the literature.

EXPERIMENTAL
Synthesis
Synthesis of MnO_x/CeO_2 catalysts
As a typical synthesis of the MnO_x/CeO_2(0.05) [where 0.05 is the theoretical Mn/(Mn + Ce) molar ratio]

Scheme 1. Synthetic and catalytic strategies for ceria-supported two-dimensional manganese oxide catalyst with strong oxide-support interactions.

catalyst, 6 g of cerium nitrate [$Ce(NO_3)_3 \cdot 6H_2O$] and 0.26 g of a manganese nitrate aqueous solution (50 wt.%) were dissolved in 5 g of ethanol and 5 g of deionized water in flask A and stirred at room temperature for 20 min. Meanwhile, 2 g of glycerol and 4.8 g of citric acid monohydrate were dissolved in 5 g of ethanol and 5 g of deionized water in flask B and stirred at room temperature for 20 min. After that, the liquor in flask B was added to flask A with continuous stirring at room temperature for 3 h and 90 °C for 3 h in a closed reactor. Finally, the ethanol and water solvent was volatilized to obtain a foamed solid. After drying at 100 °C overnight and calcining at 800 °C for 4 h in air to remove the organic species, the $MnO_x/CeO_2(0.05)$ catalyst was finally obtained. CeO_2 and $MnO_x/CeO_2(y)$ catalysts with Mn/(Mn + Ce) molar ratios of 0.025, 0.1, 0.2 and 0.3 were synthesized using the same procedure by adjusting the amount of the manganese nitrate aqueous solution in the starting solutions. Accordingly, the samples were termed as CeO_2, $MnO_x/CeO_2(0.025)$, $MnO_x/CeO_2(0.1)$, $MnO_x/CeO_2(0.2)$ and $MnO_x/CeO_2(0.3)$, respectively.

Synthesis of acid-treated $MnO_x/CeO_2(0.05)$
First, the acid-treated $MnO_x/CeO_2(0.05)$ catalyst was synthesized by washing the as-synthesized $MnO_x/CeO_2(0.05)$ with diluted hydrochloric acid (20%) at 90 °C for 4 h. The solid was then collected by centrifugation and washed with a large excess of deionized water and dried in air at 100 °C overnight. Finally, the sample was calcined in air at 400 °C for 2 h in a rotating quartz tube to obtain the acid-treated $MnO_x/CeO_2(0.05)$ catalyst.

Synthesis of MnO_x/CeO_2 and MnO_x/SiO_2
For comparison, MnO_x/CeO_2 with an Mn/(Mn + Ce) molar ratio at 0.05 was also prepared by an incipient wetness co-impregnation method. In a typical run, an $Mn(NO_3)_2$ aqueous solution (50 wt.%) was used as a precursor and CeO_2 was used as a support (CeO_2 was prepared by the citric acid-assisted method discussed above). After impregnation, the catalysts were placed in the atmosphere statically overnight and then dried in an oven and calcined at 600 °C for 4 h in air. The resulting catalyst was denoted as MnO_x/CeO_2.

MnO_x/SiO_2 was also synthesized by the same procedure for MnO_x/CeO_2 but using SiO_2 as the support.

Catalysis

Catalytic oxidation of hydrocarbons

The oxidation of hydrocarbons in the liquid phase was performed with a high-pressure autoclave reactor equipped with a magnetic stirrer (900 rpm). In a typical run, the catalyst and hydrocarbon were mixed in the reactor and pure oxygen was used for the reaction. The autoclave was purged with oxygen three times to remove the air in the autoclave before the reaction. Oxygen was then introduced to the desired pressure. Next, the reactor was rapidly heated to the desired temperature (the reaction temperature was measured by a thermocouple in the autoclave and the pressure was measured at the reaction temperature). After the reaction, the reactor was placed in an ice bath to stop the reaction, and bromobenzene or biphenyl was used as the internal standard. In the stability test, the catalyst was removed from the reactor and washed with ethanol after each reaction run, dried overnight at 150 °C and then used in the next experiment to evaluate its recyclability.

The products were analyzed by gas chromatography (GC-14C, Shimadzu, with a flame ionization detector and ethanol or acetonitrile used to dilute the liquor before the analysis) with a flexible quartz capillary column (OV-17). The gas-phase products (e.g., CO or CO_2 produced from over-oxidation) were analyzed using a Fu Li-9790 gas chromatograph equipped with a thermal conductivity detector (TCD). The as-synthesized catalyst was used each time to make sure the reactions were conducted under identical conditions. High-pressure oxygen has been extensively used in aerobic oxidations and the reaction systems in this work were out of the explosion limits of the reactants. For example, the explosion limit of ethylbenzene is 1.0%-7.1% in oxygen and the concentration of ethylbenzene in the gaseous phase in this work is out of the explosion limit. Fire and static electricity were therefore avoided for safety reasons.

Catalytic oxidation of CO

The oxidation of CO was performed in a continuous-flow fixed-bed quartz vertical reactor (length of 400 mm and internal diameter of 6 mm) in a temperature controllable oven. First, 0.2 g of catalyst (40-60 mesh) diluted with 0.6 g of quartz sands (40-60 mesh) were located in the reactor. The feed gas containing 1% CO and 18% O_2 in He was introduced with a total rate of 20 sccm. The concentration of CO in the feed and emission gases was continually monitored by the chromatograph equipped with the TCD detector. In the kinetic study, the partial pressure of CO was controlled by adjusting the flow rate of CO and the total rate was balanced with He.

Characterization

Temperature-programmed desorption

The temperature-programmed desorption of O_2 (O_2-TPD) was measured in a BELCAT II catalyst analyzer equipped with a TCD. As a typical run, 30 mg of solid catalyst were pretreated at 600 °C for 1 h in air before the measurement and then cooled to 50 °C. The sample was then heated to 800 °C at a ramp rate of 10 °C/min for detecting the desorbed oxygen species.

In-situ Fourier transform infrared spectroscopy

The *in-situ* Fourier transform infrared (FTIR) spectra were recorded using a Nicolet *is*50 FTIR spectrometer equipped with an MCT/A detector, ZnSe windows and a high temperature reaction chamber. As a typical run, 50 mg of MnO_x/CeO_2(0.05) were localized in the sample chamber and pretreated at 120 °C for 1 h in flowing Ar (30 sccm) and then cooled to room temperature. The steam containing ethylbenzene (partial pressure in the range of 9-16 mbar) was introduced into the system with a flow of Ar carrier gas (30 sccm). After adsorption for 1 h at room temperature, a pure Ar gas was introduced to purge the sample for another

1 h and the FTIR spectrum of ethylbenzene adsorbed on the solid sample was then recorded. After increasing the reaction temperature to 160 °C in flowing Ar and maintaining it for 30 min, the FTIR spectra were recorded to understand the interaction between ethylbenzene and the active oxygen species on the catalyst surface. Whilst maintaining the temperature of the chamber at 160 °C, oxygen was introduced to further promote the interaction, where the FTIR spectra were recorded to detect the formation of carbon-oxygen species.

To investigate the crucial role of the active oxygen species on the catalyst, we eliminated the oxygen by H_2 reduction during the *in-situ* FTIR study. In a typical run, 50 mg of the $MnO_x/CeO_2(0.05)$ sample were pretreated at 200 °C with 10% H_2/Ar for 2 h and then cooled to room temperature. The steam containing ethylbenzene was then introduced into the system with a flow of Ar carrier gas (30 sccm). After adsorption for 1 h at room temperature, a pure Ar gas was introduced to purge the sample for another 1 h. The FTIR spectrum of ethylbenzene adsorbed on the solid sample was then recorded. After that, the $MnO_x/CeO_2(0.05)$ catalyst was treated at 200 °C in O_2 for 1 h and then cooled to room temperature. Equivalently, ethylbenzene was introduced into the sample again and the FTIR spectrum was collected for understanding its adsorption behavior on the oxidized $MnO_x/CeO_2(0.05)$ sample. The chamber temperature was then increased to 80 °C with an oxygen flow and the FTIR spectra were recorded to characterize the interaction of ethylbenzene with the catalyst.

In-situ Raman spectroscopy
Raman spectra were recorded using an HR800 Raman spectrometer equipped with an Ar excitation source (λ = 514.532 nm). The gaseous steam was introduced into the system with a flow of Ar carrier gas (30 sccm) with the reactant partial pressure in the range of 10-20 mbar. To prove the presence of active surface oxygen species, *in-situ* Raman spectra were performed with 40 mg of the CeO_2 or $MnO_x/CeO_2(0.05)$ sample dried in a vacuum overnight to remove the water species. The Raman spectra of CeO_2 were recorded at room temperature in air. The Raman spectra of $MnO_x/CeO_2(0.05)$ were recorded at room temperature in air, room temperature in O_2, 140 °C in Ar, 250 °C in Ar, 350 °C in Ar and room temperature in O_2.

To further confirm the active surface oxygen species, *in-situ* oxidation of CO was conducted with 40 mg of the CeO_2 or $MnO_x/CeO_2(0.05)$ sample dried in a vacuum overnight to remove the water species. The Raman spectra of CeO_2 were recorded at room temperature in air. The Raman spectra of $MnO_x/CeO_2(0.05)$ were recorded at room temperature in air, room temperature in O_2, 140 °C in CO, 250 °C in CO, 350 °C in CO and 350 °C in CO and O_2.

Catalytic data analysis
Carbon balance during oxidation of hydrocarbons
The carbon balance before and after the reaction was calculated based on the number of carbon atoms in all the liquid reactants and products. For example, in the oxidation of ethylbenzene, acetophenone and phenylethyl alcohol are the detectable liquid products, while the CO_2 from over-oxidation was not included in calculating the carbon balances. The carbon balance values are calculated according to the following equation:

$$C\% = \frac{M_f*8 + M_1*n_1 + M_2*n_2 + M_3*n_3 + \ldots + M_x*n_x}{M_e*8} \times 100\%$$

where C% is the carbon balance, M_f is the final number of moles of ethylbenzene in the reactor after reaction, 8 is the number of carbon atoms in a single ethylbenzene molecule, M_1 ($M_2, M_3, ..., M_x$) is the number of moles of liquid product 1 (product 2, 3, ..., x) in the reactor after the reaction, n_1 ($n_2, n_3, ..., n_x$) is the number of carbon atoms in a single molecule of product 1 (product 2, 3, ..., x) and M_e is the number of moles of ethylbenzene in the feed mixture before the reaction.

In the kinetic study, the average reaction rates were calculated from the number of moles of substrate converted per gram of the catalyst in 1 h (mmol g_{cat}^{-1} h^{-1}) and the conversion of the reactants was controlled to be lower than 20%, which approximated the true reaction rates.

RESULTS AND DISCUSSION

Synthesis and structural characterization

The CeO_2 support was synthesized via a citric acid-assisted method [Figure 1A]. Typically, $Ce(NO_3)_3$ and citric acid were dissolved in a mixture of water, ethanol and glycerol, where the citric acid can chelate with metal ions to form the metal citrate precursor [Supplementary Figure 1]. After removing the solvent and forming a fluffy material by stirring at 90 °C, followed by calcination to remove the organic species, the CeO_2 was finally obtained [Supplementary Figure 2]. The CeO_2-supported manganese oxide catalysts were synthesized following the same procedures by adding $Mn(NO_3)_2$ in the starting solution and denoted as $MnO_x/CeO_2(y)$ [where y is the theoretical molar ratio of Mn/(Mn + Ce)] [Supplementary Figures 3-5].

Figure 1B shows the X-ray diffraction (XRD) patterns of the commercial CeO_2 and $MnO_x/CeO_2(y)$ samples with different Mn loadings, which all exhibit peaks at 28.7°, 33.3°, 47.7° and 56.5°, assigned to the (111), (200), (220) and (311) diffraction peaks of a typical CeO_2 crystal, respectively[18,22]. Notably, the shift of these diffraction peaks was undetectable for the $MnO_x/CeO_2(y)$ samples compared to the pure CeO_2, suggesting a lack of the Mn-Ce solid-solution phase[18,22]. The high dispersion and/or amorphous features of MnO_x on the CeO_2 matrix were evidenced by the undetectable XRD peaks associated with manganese oxide for $MnO_x/CeO_2(0.025)$, $MnO_x/CeO_2(0.05)$ and $MnO_x/CeO_2(0.1)$ [Figure 1C]. However, the diffraction patterns of higher Mn content samples showed the crystallization of a Mn_3O_4 hausmannite phase (JCPDS 071841)[28], demonstrating the formation of sintered MnO_x species in these samples.

The N_2 sorption demonstrates that the surface areas of CeO_2 and $MnO_x/CeO_2(0.05)$ are lower than 10 m^2/g, which should be due to the high-temperature calcination of the catalysts (800 °C for 4 h) that lead to the aggregation of the CeO_2 support and the collapse of the pore structure. The surface geometry of $MnO_x/CeO_2(0.05)$ was studied by electron microscopy characterization. As shown in Figure 2A, the bright field-scanning transmission electron microscopy image provides direct observation of the sample, showing stacked CeO_2 crystals [Supplementary Figure 6]. The Mn distribution was identified by the energy dispersive spectroscopy (EDS) elemental maps [Figure 2B-D], showing the MnO_x ensembles with diameters of 15-25 nm on the CeO_2 support, which is different from the Mn-Ce solid solution with homogeneously distributed Mn sites[18], consistent with the XRD results [Figure 1B]. Interestingly, the morphology of the MnO_x ensemble is irregular, which might suggest the amorphous structure of the MnO_x.

Figure 2E shows an enlarged view of the region in the yellow square in Figure 2A. Notably, the crystalline feature of the Mn species is completely unobservable. However, the elemental maps decidedly confirmed the existence of the MnO_x species [Figure 2F-H], demonstrating that the structural feature of $MnO_x/CeO_2(0.05)$ is mainly amorphous MnO_x on the surface of the CeO_2 matrix. The annular bright field-scanning transmission electron microscopy image with atomic resolution clearly shows the distributions of the Ce, O and Mn elements. As shown in Figure 2I-L, the ordered distributions of Ce and O are the same as
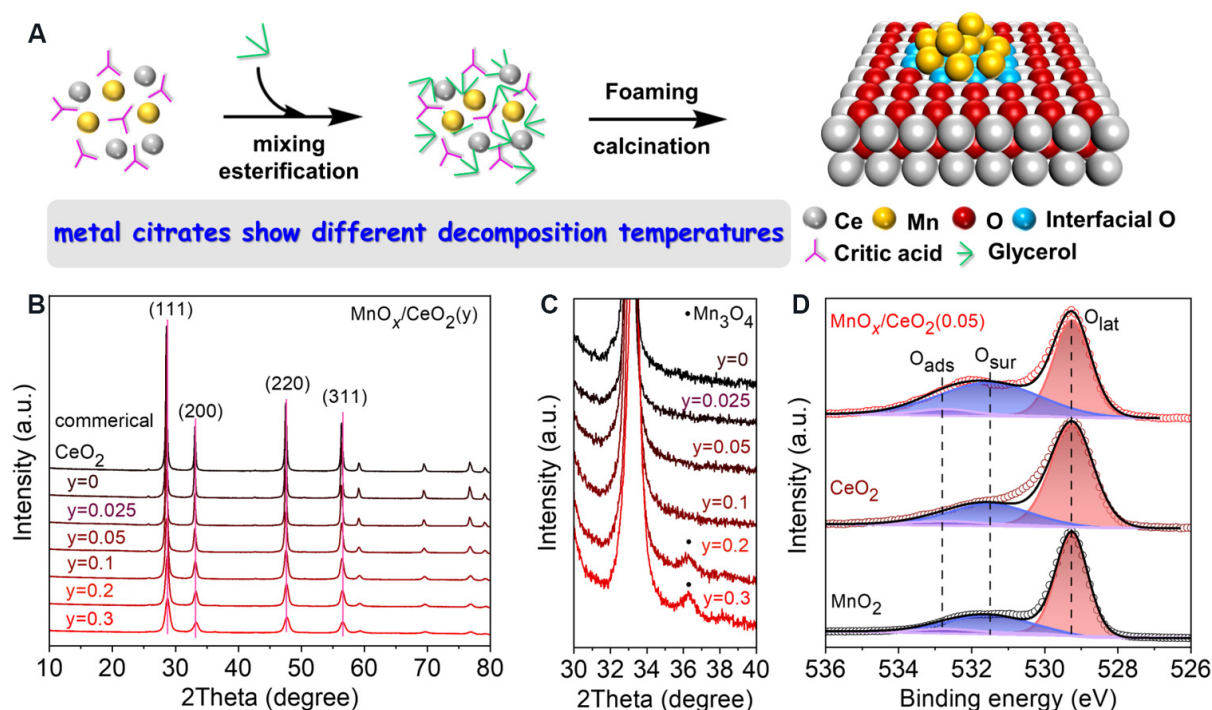
Figure 1. (A) Procedures for synthesizing $MnO_x/CeO_2(y)$ catalyst with MnO_x species anchored on the surface of ceria matrix. (B) XRD patterns of commercial CeO_2 and $MnO_x/CeO_2(y)$ catalysts with different Mn loadings. (C) Zoomed-in views of diffractions peaks in (A) from 30° to 40° for $MnO_x/CeO_2(y)$ catalysts with different Mn loadings. (D) O1s X-ray photoelectron spectra of $MnO_x/CeO_2(0.05)$, CeO_2 and MnO_2. XRD: X-ray diffraction.

those of the CeO_2 lattice. However, the random distribution of Mn confirms the amorphous feature of the MnO_x species. Significantly, the formation of an Mn-Ce solid solution is also excluded, because the smaller ionic radius of manganese ions compared to cerium ions will result in contractive lattice space in the Mn-Ce solid solution compared to the lattice space of CeO_2[18], which is not observed in this work.

The high-resolution HAADF-STEM image of the $MnO_x/CeO_2(0.05)$ catalyst directly shows that the CeO_2 matrix is partially coated with layers with an undetectable lattice [Figure 2M]. In particular, in this case, the catalyst calcined at 800 °C for 4 h precluded the carbon-containing species on the surface of CeO_2. Considering that isolated Ce sites can be found in the amorphous region [Figure 2N], it is reasonable to assign the amorphous layers to the MnO_x species. In addition, the Mn/(Mn + Ce) ratio appears at 0.22 on the catalyst surface by XPS analysis, which is distinctly different from the ratio of 0.05 in the whole oxides, indicating that MnO_x mainly exists on the CeO_2 surface. These results suggest that the structural feature of $MnO_x/CeO_2(0.05)$ is dominated by amorphous MnO_x layers on the surface of the CeO_2 matrix rather than a monophasic solid solution. The unique structure of $MnO_x/CeO_2(0.05)$ can be reasonably assigned to the citric acid-assisted method [Figure 1A], because the remarkably different decomposition temperature of cerium citrate (~161 °C) and manganese citrate (~296 °C) would benefit the phase separation to hinder the formation of the solid solution.

The MnO_x structure was further characterized by Raman and EPR measurements. As shown in Figure 2O and Supplementary Figure 7, the as-synthesized $MnO_x/CeO_2(0.05)$ catalyst shows a blue shift of the MnO_x mode (654 cm^{-1}) compared with that of various manganese oxide and supported MnO_x catalysts prepared by the conventional impregnation method (≤ 640 cm^{-1}), which is due to the SOSIs between MnO_x and the CeO_2 support and the formation of defect-rich MnO_x layers[29-31]. In contrast, the EPR spectrum of the MnO_x
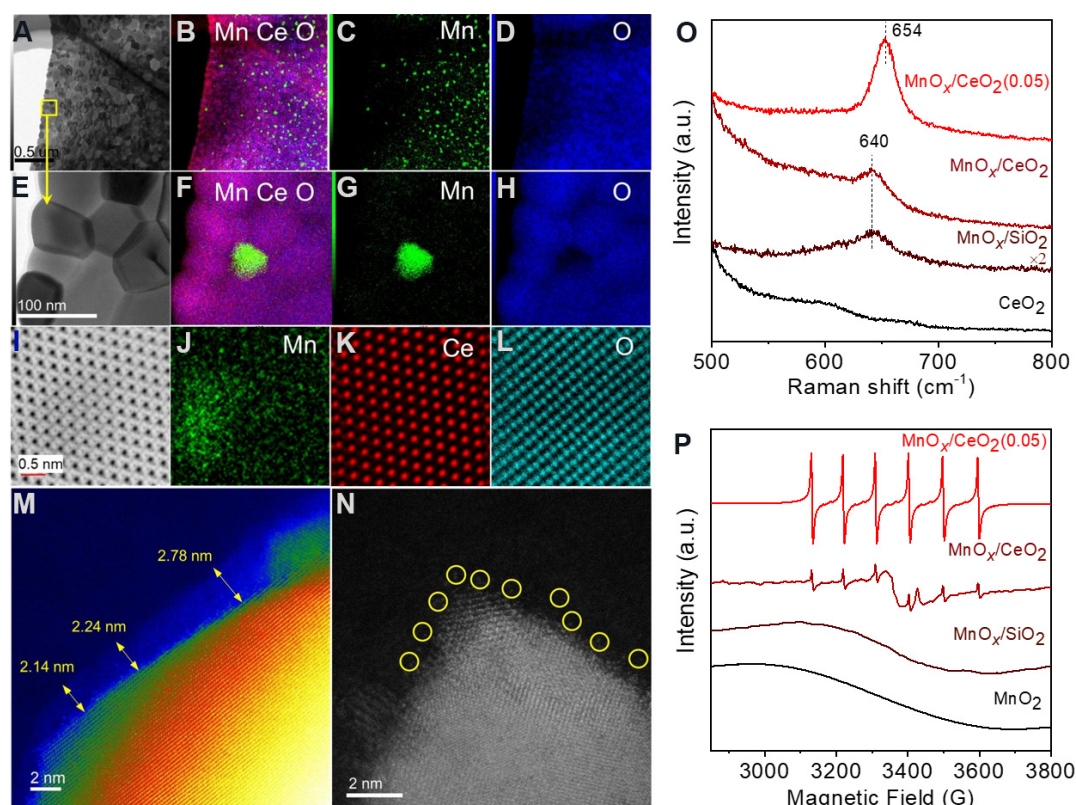
Figure 2. Electron microscopy and structural characterization. (A, E) BF-STEM images and the corresponding (B-D, F-H) Mn, Ce and O elemental maps of $MnO_x/CeO_2(0.05)$. (E) Enlarged view of the yellow square in (A). (I-L) ABF-STEM and EDS analysis of $MnO_x/CeO_2(0.05)$. (M, N) High-resolution STEM images of $MnO_x/CeO_2(0.05)$ catalyst. The isolated Ce sites in the amorphous region are highlighted by yellow circles in (N). (O) Raman and (P) EPR spectra of various samples. BF-STEM: Bright field-scanning transmission electron microscopy; ABF-STEM: annular bright field-scanning transmission electron microscopy.

$/CeO_2(0.05)$ catalyst shows sharp sextuple signals with a *g* value at 2.00 [Figure 2P], indicating the formation of abundant oxygen vacancies by loading of the MnO_x species in the $MnO_x/CeO_2(0.05)$ catalyst[32]. For comparison, the bulky manganese oxide (MnO_2), MnO_x/CeO_2 and MnO_x/SiO_2 prepared by the conventional impregnation method [Supplementary Figure 8] exhibit broad and weak signals in the EPR spectra [Figure 2P], which can be attributed to the Mn-Mn coupling (i.e., aggregation)[33-35]. These results reasonably confirmed the successful formation of well-dispersed and amorphous MnO_x layers on the surface of the ceria matrix and the construction of abundant oxygen vacancies/defective sites in the $MnO_x/CeO_2(0.05)$ catalyst, which are beneficial for the oxygen activation.

Figure 1D shows the O1s X-ray photoelectron spectra of the $MnO_x/CeO_2(0.05)$, CeO_2 and MnO_2 samples. All samples show three peaks at 529.3, 531.4 and 532.7 eV, which can be assigned to the lattice oxygen of O^{2-} (O_{lat}), surface oxygen of O_2^-, O_2^{2-} or O^- (O_{sur}) and adsorbed oxygen species from water/carbonate on the solid surface (O_{ads}), respectively[18,19,28]. In these multiple oxygen species, the surface oxygen species from the defective site with an unsaturated structure displays a key role in the oxidation, which is denoted as active oxygen[18,26]. The atomic ratio of active oxygen to the total oxygen atoms on the oxide surface of CeO_2 and MnO_2 is 26.8% and 28.4%, respectively, while the $MnO_x/CeO_2(0.05)$ exhibited a remarkably improved active oxygen capacity of 46.1% [Supplementary Table 1], which is even comparable to that of Mn-Ce solid solutions (44.1%) with a high Mn loading (50%)[18]. Considering that the $MnO_x/CeO_2(0.05)$ has a low Mn loading (5%) and is mainly presented as amorphous MnO_x layers on the CeO_2 surface, the high capacity of

active oxygen should be due to the maximized interfacial effect, causing the rich Ce^{3+} and Mn^{2+}/Mn^{3+} species [Supplementary Table 1, Figure 2P, Supplementary Figure 9] on the surface to benefit the formation of unsaturated oxygen.

Redox investigation

The redox properties of the active oxygen species on MnO_x/CeO_2(0.05) were firstly identified by the O1s X-ray photoelectron spectrum in a temperature-programmed redox cycle [Figure 3A, Supplementary Figure 10, Supplementary Table 2]. Hydrogen treatments at low temperature (room temperature to 80 °C) partially reduced the surface oxygen sites, as evidenced by the decreased intensity of the O1s peak of O_{sur} (531.4 eV) (Figure 3A and its inset), indicating that active oxygen species were available at low temperature. The subsequent reduction at the higher temperature of 120 °C led to further removal of the active oxygen. Very importantly, the active oxygen can be regenerated after treatment in air at 50 °C, displaying a similar O1s X-ray photoelectron spectrum to that of the as-synthesized sample (Figure 3A and its inset). Therefore, the high activity and remarkable stability of MnO_x/CeO_2(0.05) in the catalytic oxidation at low temperatures are reasonably expected.

Further evidence regarding the redox properties of the active oxygen species is provided by *in-situ* Raman spectroscopy. As shown in Supplementary Figure 11, MnO_x/CeO_2(0.05) gives the F_{2g} mode of the CeO_2 matrix at 460 cm^{-1}[23,30,36]. Compared to the spectrum of CeO_2, MnO_x/CeO_2(0.05) shows an additional band at 656 cm^{-1} [Figure 3B], which is associated with the Mn-O-Mn stretching mode of the surface amorphous MnO_x species with abundant defects[29-31], corresponding to the active oxygen in the X-ray photoelectron spectra [Figure 3A]. Notably, broadening, a decrease in intensity and a red shift of the band at 656 cm^{-1} occurred during the *in-situ* treatment of MnO_x/CeO_2(0.05) in atmospheric Ar at 140 °C. The intensity of the band at 645 cm^{-1} was further decreased when the temperature increased to 250 and 350 °C in Ar. This can be well explained by the desorption of the active oxygen species associated with MnO_x species to form Mn sites with more defects[20,23]. Considering the well-dispersed, amorphous and layered structure of the MnO_x species, it can be reasonably inferred that the desorption of the interfacial oxygen species accounts for the signal changes. To probe the reversibility of the active oxygen at low temperature, we exposed the sample to molecular oxygen at room temperature, resulting in a very similar Raman spectrum to the as-synthesized MnO_x/CeO_2(0.05) sample, thereby confirming the reversibility of active oxygen species [Figure 3B, Supplementary Figure 12], in good agreement with the *in-situ* XPS results [Figure 3A]. The active oxygen on MnO_x/CeO_2(0.05) was further evidenced by the O_2-TPD test [Supplementary Figure 13]. The active and reproducible oxygen species over MnO_x/CeO_2(0.05) make it a potentially efficient catalyst for aerobic oxidation reactions.

In order to support this conclusion, we further evaluated the catalytic performance of the MnO_x/CeO_2(0.05) catalyst for the CO oxidation reaction, where the activation of oxygen molecules is regarded as a key step[37,38]. Figure 4A shows the dependence of CO conversion on temperature over the MnO_x/CeO_2(0.05) and CeO_2 catalysts. The positive role of the interfacial effect on MnO_x/CeO_2(0.05) is evidenced by the full conversion of CO over MnO_x/CeO_2(0.05) at a lower temperature (270 °C) than that over CeO_2 (370 °C). By correlating the inverse of the absolute temperature (1/T) with the initial reaction rates, the apparent activation energies of MnO_x/CeO_2(0.05) and CeO_2 appeared at 51.4 and 69.2 kJ/mol, respectively [Figure 4B]. The relatively lower apparent activation energy of MnO_x/CeO_2(0.05) indicates that CO oxidation is easier. Based on the understanding that the activation energy is sensitive to the different active oxygen[37,39], a lower apparent activation energy of MnO_x/CeO_2(0.05) than that of CeO_2 should be reasonably attributed to the abundant Mn-O-Ce interfacial sites to activate O_2, rather than simply increasing the number of active oxygen species. Figure 4C shows the dependence of the reaction rate on oxygen partial pressure over different catalysts, where MnO_x/CeO_2(0.05) always displays higher reaction rates than CeO_2 at
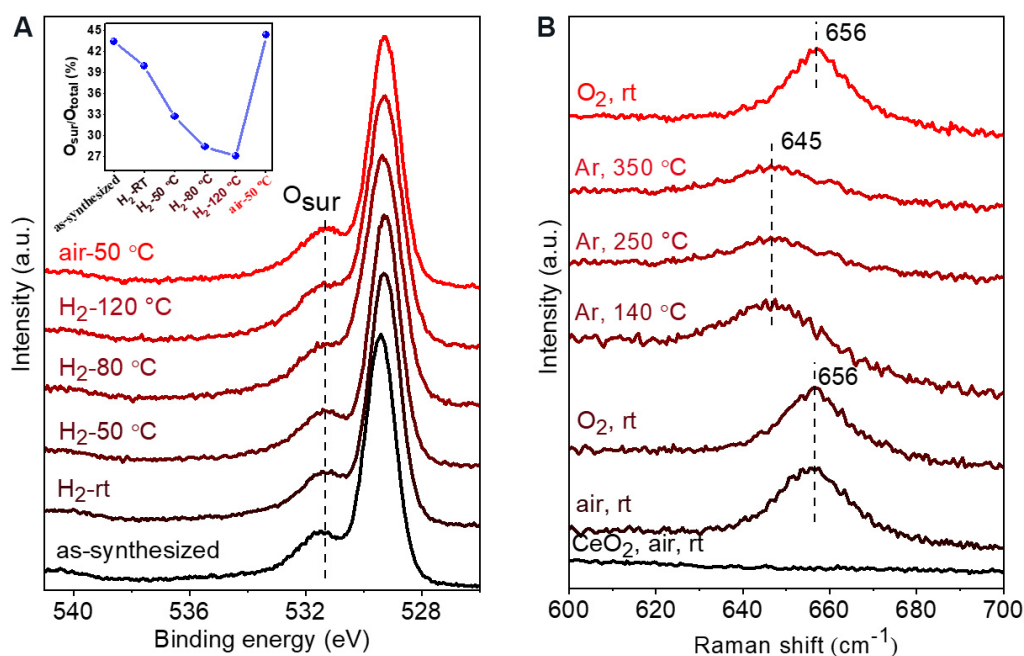
Figure 3. Redox study. (A) *In-situ* O1s X-ray photoelectron spectra of $MnO_x/CeO_2(0.05)$ under different redox conditions. Inset: the dependences of O_{sur} capacities on redox conditions. (B) *In-situ* Raman spectra of $MnO_x/CeO_2(0.05)$ and CeO_2 under different conditions.

the same oxygen pressure, thereby demonstrating its higher activities. Interestingly, under relatively low oxygen pressure (1.0-3.5 kPa), the reaction rates (r_0) over CeO_2 increased constantly with oxygen pressure, showing the reaction kinetic order at 0.37 [Figure 4D]. In contrast, the influence of oxygen pressure on the r_0 of $MnO_x/CeO_2(0.05)$ is minimal with a kinetic order at 0.04 [Figure 4D]. A lower reaction kinetic order suggests that the activity of $MnO_x/CeO_2(0.05)$ is insensitive to the oxygen pressure[37,40], which is reasonably attributed to the enhanced ability of the well-dispersed and amorphous MnO_x species in $MnO_x/CeO_2(0.05)$ to activate molecular oxygen efficiently. These results indicate that the proof-of-concept design of the catalyst benefits the enhancement of catalytic efficacy in aerobic oxidations.

Aerobic oxidation of hydrocarbons
Initial attempts to evaluate the catalysts were performed in the selective oxidation of ethylbenzene to acetophenone and 1-phenylethanol at a low temperature of 110 °C for 6 h without solvent and initiator additives [Table 1]. A higher molar ratio of acetophenone and 1-phenylethanol indicates the deep dehydrogenation of 1-phenylethanol to acetophenone. The blank run without catalysts showed undetected reactivity (entry 1). The commercial nanosized CeO_2, MnO_2 and CeO_2 were active for the reaction, giving ethylbenzene conversion at 3.0%, 1.3% and 6.8%, respectively (entries 2-4). The Mn salts of $MnCl_2$ and $KMnO_4$, which are well-known homogeneous catalysts in oxidation, gave ethylbenzene conversion at 8.2% and 1.9%, respectively (entries 5 and 6). Interestingly, interfacing MnO_x on CeO_2 significantly influenced the catalytic activity, where enhanced conversions were achieved over the MnO_x/CeO_2 catalysts (entries 7-11). By optimizing the Mn loadings on the catalysts, the best performance was achieved over $MnO_x/CeO_2(0.05)$ with the highest capacity of active surface oxygen, displaying ethylbenzene conversion at 12.9% (entry 8). The decreased activity for the MnO_x/CeO_2 catalysts with an Mn/(Mn + Ce) ratio higher than 0.05 is due to the aggregation of the MnO_x species [Figure 1C], leading to limited Mn-O-Ce interfacial sites for the oxidation of substrates. Very interestingly, the oxidation of ethylbenzene can be performed at a low temperature at 70 °C (entry 14), demonstrating the superior catalytic activity of $MnO_x/CeO_2(0.05)$.

Table 1. Catalytic data in oxidation of ethylbenzene[a]

Entry	Catalyst	Temp. (°C)	Time (h)	Conv. (%)	Sel. (%)	A/P[b]
1	Blank	110.0	6.0	< 0.1	n.d.	n.d.
2	Commercial CeO_2	110.0	6.0	3.0	> 99.0	0.8
3	MnO_2	110.0	6.0	1.3	> 99.0	0.6
4	CeO_2	110.0	6.0	6.8	> 99.0	1.1
5[c]	$MnCl_2$	110.0	6.0	8.2	97.6	2.6
6[c]	$KMnO_4$	110.0	6.0	1.9	94.7	2.0
7	$MnO_x/CeO_2(0.025)$	110.0	6.0	9.2	> 99.0	1.2
8	$MnO_x/CeO_2(0.05)$	110.0	6.0	12.9	> 99.0	1.9
9	$MnO_x/CeO_2(0.1)$	110.0	6.0	7.1	> 99.0	0.7
10	$MnO_x/CeO_2(0.2)$	110.0	6.0	5.6	> 99.0	0.4
11	$MnO_x/CeO_2(0.3)$	110.0	6.0	4.1	> 99.0	0.5
12	$MnO_x/CeO_2(0.05)$	110.0	16.0	27.1	> 99.0	2.1
13	$MnO_x/CeO_2(0.05)$	110.0	24.0	29.4	> 99.0	2.6
14	$MnO_x/CeO_2(0.05)$	70.0	6.0	0.7	> 99.0	0.8
15	$MnO_x/CeO_2(0.05)$	90.0	6.0	4.3	> 99.0	1.5
16	$MnO_x/CeO_2(0.05)$	130.0	6.0	24.2	> 99.0	2.0
17	$MnO_x/CeO_2(0.05)$	130.0	24.0	34.7	> 99.0	1.9
18	$MnO_x/CeO_2(0.05)$, 200 mg	130.0	24.0	52.8	> 99.0	3.4
19	$MnO_x/CeO_2(0.05)$, 400 mg	130.0	24.0	59.2	> 99.0	7.0
20	$MnO_x/CeO_2(0.05)$, 400 mg, 3 MPa of O_2	130.0	24.0	63.5	95.7	5.8
21	$MnO_x/CeO_2(0.05)$, 600 mg, 3 MPa of O_2	130.0	24.0	65.6	77.6	4.7
22[d]	MnO_x/CeO_2	130.0	24.0	19.2	> 99.0	16
23	$MnO_x/CeO_2(0.05)$, 2 MPa of N_2	110.0	6.0	< 0.1	n.d.	n.d.
24	$MnO_x/CeO_2(0.05)$, 50 mg of hydroquinone	110.0	6.0	< 0.1	n.d.	n.d.

[a]Reaction conditions: 47 mmol of substrate, 100 mg of catalyst, 2.0 MPa of oxygen; [b]A/P: molar ratio of acetophenone and 1-phenylethanol; [c]Molar weight of the Mn in the catalyst is the same as the molar weight of Mn in $MnO_x/CeO_2(0.05)$; [d]Catalyst prepared from conventional impregnation method. Conv.: Conversion; Sel.: selectivity to acetophenone and 1-phenylethanol; n.d.: not detected.

To realize the best performance, we optimized the reaction temperature, time, catalyst amount and oxygen pressure in the reactor (entries 12-21). The ethylbenzene conversion of 59.2% with > 99.0% selectivity to acetophenone and 1-phenylethanol was achieved (entry 19). This result, obtained under solvent- and initiator-free conditions, even outperforms a series of superior catalysts for C-H bond selective oxidations reported in the literature [Supplementary Table 3], such as the Au nanosheet with undetectable reactivity under solvent- and initiator-free conditions[12]. The MnO_x/CeO_2 catalyst synthesized from the conventional impregnation method with the same Mn loading to $MnO_x/CeO_2(0.05)$ exhibited poor activity (entry 22), which might be due to the aggregation of the MnO_x particles and the limited interfacial sites, as confirmed by the Raman and EPR analysis [Figure 2O and P]. Increasing the $MnO_x/CeO_2(0.05)$ catalyst amount led to enhanced ethylbenzene conversion but unsatisfactory carbon balance values because of the over-oxidation to CO and CO_2 (entries 20 and 21, Supplementary Figure 14). The molecular oxygen indeed acted as oxygen donors in the reaction, as evidenced by the undetectable conversion of ethylbenzene when using nitrogen instead of oxygen in the reaction (entry 23). When the free radical scavenger was added to the reaction system, the reaction was quenched, demonstrating that the reaction follows a radical chain mechanism (entry 24).

More importantly, the catalyst is stable, reusable and can be easily filtrated and recycled after each reaction run. Consequently, it exhibited stable catalytic performance in the recycling tests
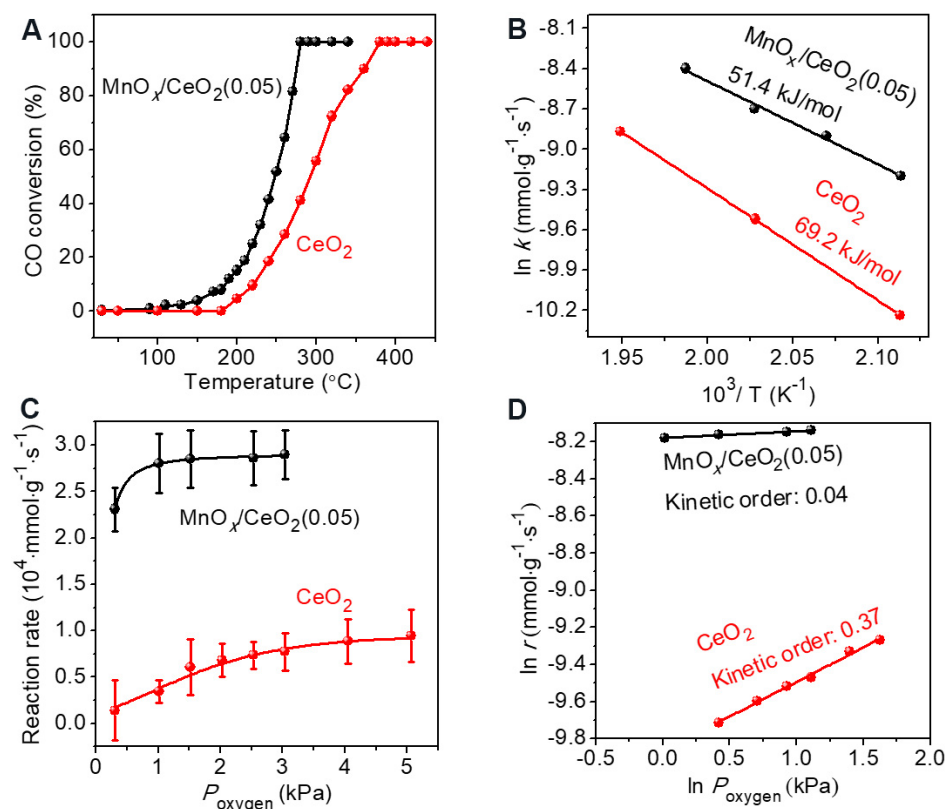
Figure 4. CO oxidation. (A) Dependence of CO conversion on temperature over $MnO_x/CeO_2(0.05)$ and CeO_2 catalysts. (B) Arrhenius plots of CO oxidation over $MnO_x/CeO_2(0.05)$ and CeO_2 catalysts. (C) Dependence of reaction rate on oxygen pressure in CO oxidation over $MnO_x/CeO_2(0.05)$ and CeO_2 catalysts. (D) Data characterizing the kinetic reaction order of oxygen in CO oxidation over $MnO_x/CeO_2(0.05)$ and CeO_2 catalysts.

[Supplementary Figure 15]. In the six runs of selective ethylbenzene oxidation, the $MnO_x/CeO_2(0.05)$ catalyst exhibited constant conversion and selectivity, indicating good recyclability and stability. Notably, the $MnO_x/CeO_2(0.05)$ catalyst is generally effective for the selective oxidation of various phenolic hydrocarbons [Supplementary Table 4], giving desired products with good activities and selectivities. It is noteworthy that these reactions were all performed under solvent- and initiator-free conditions, which make the $MnO_x/CeO_2(0.05)$ catalyst potentially useful for wide applications in the selective oxidation of C-H bonds.

Mechanism investigation

Based on the aforementioned results, we conclude that $MnO_x/CeO_2(0.05)$ is highly active for the selective oxidation of C-H bonds under solvent- and initiator-free conditions at low temperature based on its earth-abundant metals as catalysts and constructing SOSIs. In contrast to the existing understanding that highly active Mn-Ce catalysts should be dominated by the solid-solution phase, the greatest difference in our case is that $MnO_x/CeO_2(0.05)$ has separated phases of two-dimensional and amorphous MnO_x layers on CeO_2. We conclude that the high efficacy of $MnO_x/CeO_2(0.05)$ originates from the SOSIs and maximized interfacial effects, because a highly active solid-solution catalyst requires a high Mn concentration (~50%)[18].

In order to further address this conclusion, we performed acid treatment for $MnO_x/CeO_2(0.05)$ to partially remove the surface MnO_x species, as confirmed by the X-ray photoelectron spectra giving the surface Mn/(Mn + Ce) ratio decreased from 0.22 to almost undetectable [Figure 5A]. The acid-treated
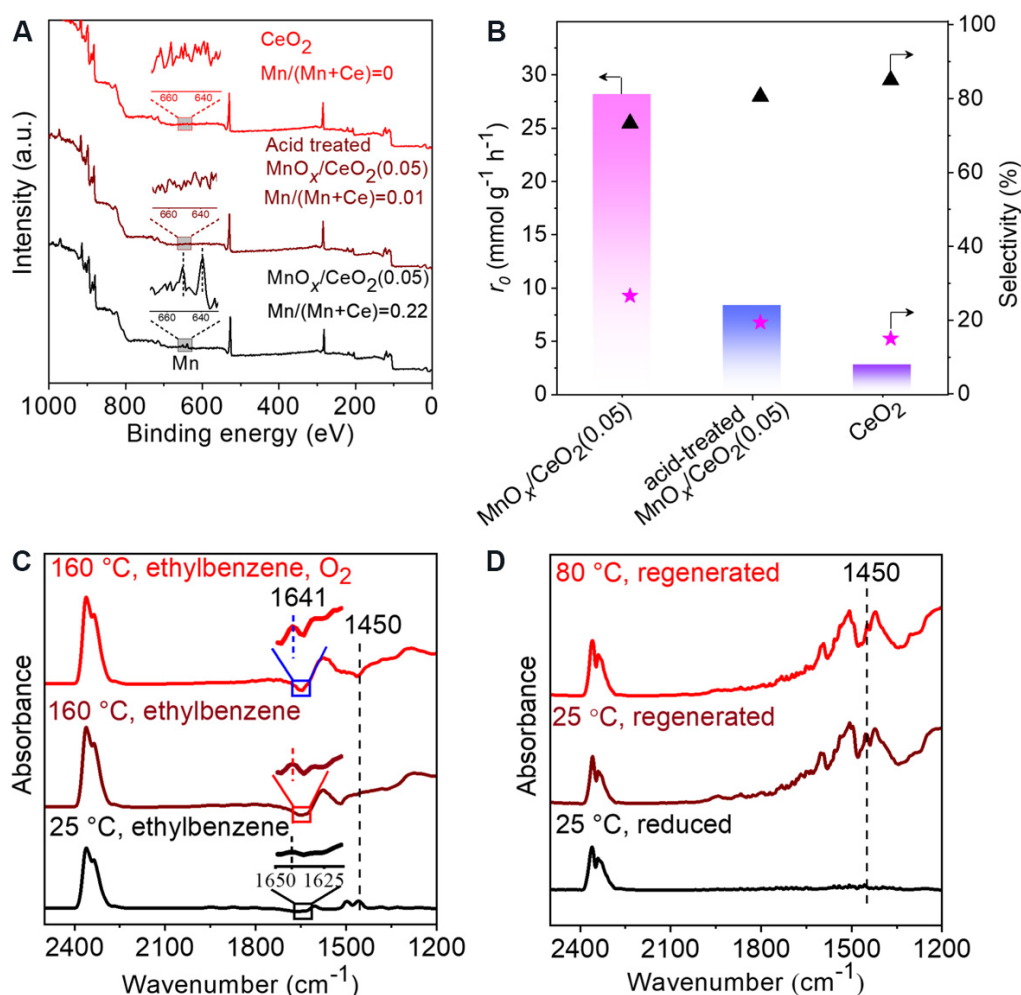
Figure 5. Mechanism studies. (A) X-ray photoelectron spectra of $MnO_x/CeO_2(0.05)$, acid-treated $MnO_x/CeO_2(0.05)$ and CeO_2. (B) Reaction rate and product selectivities in ethylbenzene oxidation over various catalysts. The triangles and stars represent the selectivities to 1-phenylethanol and acetophenone, respectively. (C) *In-situ* FTIR spectra of ethylbenzene adsorbed on $MnO_x/CeO_2(0.05)$ at 25 and 160 °C in flowing Ar and then switched to O_2. (D) *In-situ* FTIR spectra of ethylbenzene adsorbed on H_2-reduced $MnO_x/CeO_2(0.05)$ at 25 °C, O_2-regenerated $MnO_x/CeO_2(0.05)$ at 25 °C and 80 °C. FTIR: Fourier transform infrared.

$MnO_x/CeO_2(0.05)$ exhibited a significantly reduced ethylbenzene conversion rate (8 mmol g^{-1} h^{-1}) compared to the fresh catalyst (28 mmol g^{-1} h^{-1}) [Figure 5B] under equivalent reaction conditions, demonstrating the important role of the surface MnO_x species of $MnO_x/CeO_2(0.05)$ in generating abundant interfacial active sites. In order to understand the role of active oxygen on $MnO_x/CeO_2(0.05)$ for C-H bond oxidation, we performed *in-situ* FTIR spectroscopy studies of C-H bond oxidation. Figure 5C shows the ethylbenzene-adsorption FTIR spectrum of $MnO_x/CeO_2(0.05)$, which gives the typical peak at 1450 cm^{-1} assigned to the C-H bond[18]. By increasing the temperature to 160 °C in flowing Ar, the C-H peak was remarkably weakened, which should be due to the activation of the C-H bond by the surface oxygen species on the $MnO_x/CeO_2(0.05)$ catalyst, because the hydrocarbon favors reacting with the active surface oxygen with an asymmetric Coulombic interaction with Mn and Ce[18,20]. Meanwhile, the readily observed C=O bond at 1641 cm^{-1} confirmed that the C-H bonds are indeed oxidized by the active oxygen on the solid surface into C=O species[18]. The introduction of external molecular oxygen further enhanced the transformation of the C-H bonds at 160 °C, as evidenced by the increased intensity of the C=O peak at 1641 cm^{-1}.

The aforementioned results demonstrate the important role of the active oxygen species on the $MnO_x/CeO_2(0.05)$ catalyst in activating C-H bonds. After purging $MnO_x/CeO_2(0.05)$ with hydrogen to reduce the active oxygen at 200 °C, the system was switched to the Ar flow with ethylbenzene molecules at 25 °C. The reduced $MnO_x/CeO_2(0.05)$ failed to adsorb ethylbenzene, as confirmed by the undetectable peak of C-H bonds in the *in-situ* FTIR spectrum [Figure 5D]. Furthermore, after regeneration of the active oxygen, the adsorption of C-H bonds occurred again on the regenerated catalyst at 25 °C. Increasing the temperature to 80 °C led to a significant weakening of the C-H bonds, confirming that they were readily activated by the regenerated active oxygen species. These phenomena demonstrate the important role of active oxygen in the adsorption and activation of C-H bonds.

CONCLUSIONS

In summary, we have demonstrated a ceria-supported two-dimensional manganese oxide with a SOSI effect as an efficient catalyst for the selective oxidation of hydrocarbons, thereby breaking the normal principle of synthesizing Mn-Ce catalysts with an abundant solid-solution phase. The key to the success is to anchor well-dispersed and amorphous MnO_x layers on the CeO_2 matrix by SOSIs, forming abundant active oxygen species over $MnO_x/CeO_2(0.05)$ because of the high interfacial efficacy, which displays crucial roles in the adsorption and activation of C-H bonds. In the selective oxidation of hydrocarbons to the corresponding alcohols and ketones, $MnO_x/CeO_2(0.05)$ exhibited high activity, selectivity and recyclability under solvent- and initiator-free conditions at low temperature, outperforming the noble catalysts and the state-of-the-art Mn-Ce metal oxide catalysts. This work not only highlights the importance of SOSIs for the oxidation of C-H bonds but also extends the principle for designing efficient metal oxide catalysts for the sustainable production of valuable chemicals.

DECLARATIONS

Authors' contributions
Carried out the catalyst preparation, characterization, catalytic tests, and prepared the draft manuscript: Wang H
Performed part of the catalyst characterization: Luo Q, Zhang J, Wang C
Performed the TEM characterization: Ge X, Zhang W
Planned the study, analysed the data and wrote the manuscript: Wang L, Xiao FS

Availability of data and materials
Experimental details on materials and characterization are available in the Supplementary Information, and the data supporting the findings of this study are available from the corresponding author upon reasonable request.

Conflict of interest
All authors declared that there are no conflicts of interest.

Ethical approval and consent to participate
Not applicable.

Consent for publication

Not applicable.

Copyright

© The Author(s) 2022.

REFERENCES

1.   White MC. Chemistry. Adding aliphatic C-H bond oxidations to synthesis. *Science* 2012;335:807-9. DOI PubMed

2.   ten Brink GJ, Arends IW, Sheldon RA. Green, catalytic oxidation of alcohols in water. *Science* 2000;287:1636-9. DOI PubMed

3.   Marimuthu A, Zhang J, Linic S. Tuning selectivity in propylene epoxidation by plasmon mediated photo-switching of Cu oxidation state. *Science* 2013;339:1590-3. DOI PubMed

4.   Liu W, Zhang L, Liu X, et al. Discriminating catalytically active FeN$_x$ species of atomically dispersed Fe-N-C catalyst for selective oxidation of the C-H bond. *J Am Chem Soc* 2017;139:10790-8. DOI PubMed

5.   Kulangiappar K, Anbu Kulandainathan M, Raju T. Conversion of benzylic bromides to benzaldehydes using sodium nitrate as an oxidant. *Ind Eng Chem Res* 2010;49:6670-3. DOI

6.   Frei H. Chemistry. Selective hydrocarbon oxidation in zeolites. *Science* 2006;313:309-10. DOI PubMed

7.   Hughes MD, Xu YJ, Jenkins P, et al. Tunable gold catalysts for selective hydrocarbon oxidation under mild conditions. *Nature* 2005;437:1132-5. DOI PubMed

8.   Pradhan S, Bartley JK, Bethell D, et al. Non-lattice surface oxygen species implicated in the catalytic partial oxidation of decane to oxygenated aromatics. *Nat Chem* 2012;4:134-9. DOI PubMed

9.   Yuan C, Liang Y, Hernandez T, Berriochoa A, Houk KN, Siegel D. Metal-free oxidation of aromatic carbon-hydrogen bonds through a reverse-rebound mechanism. *Nature* 2013;499:192-6. DOI PubMed

10. Zope BN, Hibbitts DD, Neurock M, Davis RJ. Reactivity of the gold/water interface during selective oxidation catalysis. *Science* 2010;330:74-8. DOI PubMed

11. Fu Q, Li WX, Yao Y, et al. Interface-confined ferrous centers for catalytic oxidation. *Science* 2010;328:1141-4. DOI PubMed

12. Wang L, Zhu Y, Wang JQ, et al. Two-dimensional gold nanostructures with high activity for selective oxidation of carbon-hydrogen bonds. *Nat Commun* 2015;6:6957. DOI PubMed PMC

13. Liu Y, Tsunoyama H, Akita T, Xie S, Tsukuda T. Aerobic oxidation of cyclohexane catalyzed by size-controlled Au clusters on hydroxyapatite: size effect in the sub-2 nm regime. *ACS Catal* 2011;1:2-6. DOI

14. Turner M, Golovko VB, Vaughan OP, et al. Selective oxidation with dioxygen by gold nanoparticle catalysts derived from 55-atom clusters. *Nature* 2008;454:981-3. DOI PubMed

15. Neufeldt SR, Sanford MS. Controlling site selectivity in palladium-catalyzed C-H bond functionalization. *Acc Chem Res* 2012;45:936-46. DOI PubMed PMC

16. Muzart J. Ionic liquids as solvents for catalyzed oxidations of organic compounds. *Adv Synth Catal* 2006;348:275-95. DOI

17. Qi G, Yang RT, Chang R. MnO$_x$-CeO$_2$ mixed oxides prepared by co-precipitation for selective catalytic reduction of NO with NH$_3$ at low temperatures. *Appl Catal B* 2004;51:93-106. DOI

18. Zhang P, Lu H, Zhou Y, et al. Mesoporous MnCeO$_x$ solid solutions for low temperature and selective oxidation of hydrocarbons. *Nat Commun* 2015;6:8446. DOI PubMed PMC

19. Venkataswamy P, Rao KN, Jampaiah D, Reddy BM. Nanostructured manganese doped ceria solid solutions for CO oxidation at lower temperatures. *Appl Catal B* 2015;162:122-32. DOI

20. Zou Z, Meng M, Zha Y. Surfactant-assisted synthesis, characterizations, and catalytic oxidation mechanisms of the mesoporous MnO$_x$-CeO$_2$ and Pd/MnO$_x$-CeO$_2$ catalysts used for CO and C$_3$H$_8$ oxidation. *J Phys Chem C* 2010;114:468-77. DOI

21. Elias JS, Risch M, Giordano L, Mansour AN, Shao-Horn Y. Structure, bonding, and catalytic activity of monodisperse, transition-metal-substituted CeO$_2$ nanoparticles. *J Am Chem Soc* 2014;136:17193-200. DOI PubMed

22. Wang C, Wen C, Lauterbach J, Sasmaz E. Superior oxygen transfer ability of Pd/MnO$_x$-CeO$_2$ for enhanced low temperature CO oxidation activity. *Appl Catal B* 2017;206:1-8. DOI

23. Zhang X, Deng Y, Tian P, Shang H, Xu J, Han Y. Dynamic active sites over binary oxide catalysts: In situ/operando spectroscopic study of low-temperature CO oxidation over MnO$_x$-CeO$_2$ catalysts. *Appl Catal B* 2016;191:179-91. DOI

24. Delimaris D, Ioannides T. VOC oxidation over MnO$_x$-CeO$_2$ catalysts prepared by a combustion method. *Appl Catal B* 2008;84:303-12. DOI

25. Cen W, Liu Y, Wu Z, Wang H, Weng X. A theoretic insight into the catalytic activity promotion of CeO$_2$ surfaces by Mn doping. *Phys Chem Chem Phys* 2012;14:5769-77. DOI PubMed

26. Wang Z, Shen G, Li J, Liu H, Wang Q, Chen Y. Catalytic removal of benzene over CeO$_2$-MnO$_x$ composite oxides prepared by hydrothermal method. *Appl Catal B* 2013;138-139:253-9. DOI

27. Tang X, Chen J, Huang X, Xu Y, Shen W. Pt/MnO$_x$-CeO$_2$ catalysts for the complete oxidation of formaldehyde at ambient temperature. *Appl Catal B* 2008;81:115-21. DOI

28. Quiroz J, Giraudon J, Gervasini A, et al. Total oxidation of formaldehyde over MnO$_x$-CeO$_2$ catalysts: the effect of acid treatment. *ACS Catal* 2015;5:2260-9. DOI

29. Li X, Lunkenbein T, Pfeifer V, et al. Selective alkane oxidation by manganese oxide: site isolation of MnO$_x$ chains at the surface of

MnWO$_4$ nanorods. *Angew Chem Int Ed Engl* 2016;55:4092-6. DOI PubMed

30. Lin X, Li S, He H, et al. Evolution of oxygen vacancies in MnO$_x$-CeO$_2$ mixed oxides for soot oxidation. *Appl Catal B* 2018;223:91-102. DOI

31. Xu J, Li P, Song X, He C, Yu J, Han Y. Operando raman spectroscopy for determining the active phase in one-dimensional Mn$_{1-x}$Ce$_x$O$_{2\pm y}$ nanorod catalysts during methane combustion. *J Phys Chem Lett* 2010;1:1648-54. DOI

32. Figaj M, Becker K. An electron paramagnetic resonance study of impurities in ceria, CeO$_2$. *Solid State Ionics* 2001;141-142:507-12. DOI

33. Yang X, Pu C, Qin H, Liu S, Xu Z, Peng X. Temperature- and Mn^{2+} concentration-dependent emission properties of Mn^{2+}-doped ZnSe nanocrystals. *J Am Chem Soc* 2019;141:2288-98. DOI PubMed

34. Kurz T, Chen L, Brieler FJ, et al. Minimal number of atoms to constitute a magnet: Suppression of magnetic order in spherical MnS nanoparticles. *Phys Rev B* 2008;78:132408. DOI

35. Goede O, Backs D, Heimbrodt W, Kanis M. EPR study of the antiferromagnetic phase transition in (Cd, Mn)S. *phys stat sol (b)* 1989;151:311-8. DOI

36. Sato T, Komanoya T. Selective oxidation of alcohols with molecular oxygen catalyzed by Ru/MnO/CeO$_2$ under mild conditions. *Catalysis Communications* 2009;10:1095-8. DOI

37. Xie X, Li Y, Liu ZQ, Haruta M, Shen W. Low-temperature oxidation of CO catalysed by Co(3)O(4) nanorods. *Nature* 2009;458:746-9. DOI PubMed

38. Chen G, Zhao Y, Fu G, et al. Interfacial effects in iron-nickel hydroxide-platinum nanoparticles enhance catalytic oxidation. *Science* 2014;344:495-9. DOI PubMed

39. Gu D, Tseng JC, Weidenthaler C, et al. Gold on different manganese oxides: ultra-low-temperature CO oxidation over colloidal gold supported on bulk-MnO$_2$ nanomaterials. *J Am Chem Soc* 2016;138:9572-80. DOI PubMed

40. Yu WZ, Wang WW, Li SQ, et al. Construction of active site in a sintered copper-ceria nanorod catalyst. *J Am Chem Soc* 2019;141:17548-57. DOI PubMed